

Seamless Immersed Boundary Lattice Boltzmann Method for Incompressible Flow Simulation

H. Nishida* and Y. Meichin*
Corresponding author: nishida@kit.ac.jp

* Kyoto Institute of Technology, JAPAN.

Abstract: In this paper, the seamless immersed boundary lattice Boltzmann method is proposed, in order to simulate the complicated incompressible flows on the Cartesian grid. The present approach is an extension of the seamless immersed boundary method for the incompressible Navier-Stokes equations to the lattice Boltzmann equation. In the seamless immersed boundary method for solving the Navier-Stokes equations, the forcing term which satisfies the velocity condition on the virtual boundary is added not only to the grid points near the boundary but also to the grid points inside the boundary, so that the pressure profile near the boundary becomes smoothly. Similarly in the present method, the external forcing function is added to the lattice Boltzmann equation. The present method is validated for the typical benchmark flows, e.g., flow around a circular cylinder and flow around a moving circular cylinder. As a result, it is confirmed that the present method gives the smooth pressure field without the unphysical oscillation and pressure jump near the boundary. Then, it is concluded that the present seamless immersed boundary lattice Boltzmann method is very versatile for simulating the complicated incompressible flows.

Keywords: Lattice Boltzmann Method, Seamless Immersed Boundary Method, Incompressible Flow Simulation.

1 Introduction

In the incompressible flow simulation, the lattice Boltzmann method is spotlighted as an alternative computational approach for solving the Navier-Stokes equations. In today's parallel computer architecture progress, it is expected that this trend continues because the lattice Boltzmann method is suitable for parallelization. However, the lattice Boltzmann method originally assumes that the particles move on the rectangular grid (lattice). This is the weak point of the method for simulating the complicated flow field with curved geometry. For improving the weak point, mainly two approaches are proposed. One is the proposals of suitable boundary condition for curved boundary [1, 2, 3, 4, 5, 6, 7]. These curved boundary conditions are achieving good results, but the intricate boundary treatment is necessary for more complicated flow geometry.

Another approach is the combination of lattice Boltzmann method and immersed boundary method. The immersed boundary method was first proposed by Peskin [8] for simulating the blood flow in the heart. This approach is calculation including inside the boundary on the Cartesian grid. Recently, Goldstein et al. [9] and Saiki and Biringen [10] developed the continuous (feedback) forcing treatment. Afterwards, Fadlun et al. [11] proposed the discrete (direct) forcing treatment. In these approaches, the external forcing term which satisfies the velocity condition on the virtual boundary is added to the governing momentum equations, i.e., the Navier-Stokes equations. Also, the extension to the energy equation was developed by Nishida [12]. The immersed boundary method is extended to the lattice Boltzmann method [13, 14, 15, 16, 17, 18].

In the Navier-Stokes equation solver, however, the conventional external forcing term is added only on the grid points near the virtual boundary. The resulting pressure profile has the pressure jump near the virtual boundary, so that the unphysical oscillation appears near the virtual boundary. Then, it is difficult to estimate the precise quantities, i.e., pressure near the boundary. In order to remove the unphysical

oscillation, Nishida et al. [19, 20] proposed the seamless immersed boundary method. In the seamless immersed boundary method, the external forcing term is added not only to the grid points near the virtual boundary but also to the grid points inside the virtual boundary. As a result, the unphysical oscillation disappears and the smooth pressure field can be obtained. Also, the seamless immersed boundary method is applied to the flow with heat transfer [21] and the curvilinear coordinates [22], successfully.

In this paper, we try to combine the seamless immersed boundary method with the lattice Boltzmann method. A new seamless immersed boundary lattice Boltzmann method is validated for some benchmark flow fields, e.g., flow around a circular cylinder and flow around a moving circular cylinder. And we discuss the property of seamless immersed boundary lattice Boltzmann method.

2 Seamless Immersed Boundary Lattice Boltzmann Method

2.1 Lattice Boltzmann method

The lattice Boltzmann method is constructed by the collision and advection of the fluid particle. The lattice Boltzmann equation with the single relaxation time approximation is written by

$$f_\alpha(\mathbf{x} + \mathbf{e}_\alpha \Delta t, t + \Delta t) - f_\alpha(\mathbf{x}, t) = \Omega_\alpha, \quad (1)$$

where Ω_α denotes the collision term. By using the Bhatnagar-Gross-Krook (BGK) approximation for the collision term, the following lattice Boltzmann equation can be obtained.

$$f_\alpha(\mathbf{x} + \mathbf{e}_\alpha \Delta t, t + \Delta t) - f_\alpha(\mathbf{x}, t) = -\frac{1}{\tau} \left[f_\alpha(\mathbf{x}, t) - f_\alpha^{(eq)}(\mathbf{x}, t) \right]. \quad (2)$$

In the $D2Q9$ model [23], the discrete velocity \mathbf{e}_α is defined by

$$\mathbf{e}_\alpha = \begin{cases} (0, 0), & (\alpha = 0) \\ \left(\cos \left[\frac{(\alpha-1)\pi}{2} \right], \sin \left[\frac{(\alpha-1)\pi}{2} \right] \right), & (\alpha = 1 \sim 4) \\ \sqrt{2} \left(\cos \left[\frac{(2\alpha-9)\pi}{4} \right], \sin \left[\frac{(2\alpha-9)\pi}{4} \right] \right), & (\alpha = 5 \sim 8) \end{cases}, \quad (3)$$

where f_α denotes the distribution function, α ($= 0 \sim 8$) is the moving direction, \mathbf{x} is the location, and τ is the single relaxation time. The equilibrium distribution function, $f_\alpha^{(eq)}$, in Eq.(2) is determined by

$$f_\alpha^{(eq)} = w_\alpha \rho \left[1 + \frac{1}{c_s^2} (\mathbf{e}_\alpha \cdot \mathbf{u}) + \frac{1}{2c_s^4} (\mathbf{e}_\alpha \cdot \mathbf{u})^2 - \frac{1}{2c_s^2} \mathbf{u}^2 \right], \quad (4)$$

where w_α ($= 4/9$ ($\alpha = 0$), $1/9$ ($\alpha = 1 \sim 4$), $1/36$ ($\alpha = 5 \sim 8$)) is the weighted coefficients and \mathbf{u} the velocity vector. $c_s = 1/\sqrt{3}$ is the speed of sound. The kinematic viscosity is related to the single relaxation time τ as $\nu = (2\tau - 1)\Delta t/6$ [24]. The macroscopic pressure and velocity are computed by

$$p = \rho c_s^2 = c_s^2 \sum_\alpha f_\alpha, \quad \rho \mathbf{u} = \sum_\alpha f_\alpha \cdot \mathbf{e}_\alpha. \quad (5)$$

By using the Chapman-Enskog expansion, the lattice Boltzmann equation (2) is equivalent to the fluid equations, i.e., the Navier-Stokes equations.

2.2 Seamless immersed boundary method

2.2.1 Immersed boundary method

In the immersed boundary method, the practical boundary, i.e., object surface or flow pass, is expressed by the virtual boundary. The velocity conditions on the virtual boundary are satisfied by adding the forcing term to the momentum equations. Then, the incompressible viscous flow is governed by the continuity equation and the incompressible Navier-Stokes equations. These equations can be written in the non-dimensional

form by

$$\frac{\partial u_i}{\partial x_i} = 0 \quad , \quad (6)$$

$$\frac{\partial u_i}{\partial t} + u_j \frac{\partial u_i}{\partial x_j} = -\frac{\partial p}{\partial x_i} + \frac{1}{Re} \frac{\partial^2 u_i}{\partial x_j \partial x_j} + G_i \quad , \quad (7)$$

where u_i and p denote the velocity component and the pressure. $Re(= \overline{U}\overline{L}/\overline{\nu})$ denotes the Reynolds number. \overline{U} , \overline{L} , and $\overline{\nu}$ are the reference velocity, the reference length, and the kinematic viscosity, respectively. The last term in Eq.(7), G_i , denotes the additional forcing term for the immersed boundary method.

In order to estimate the additional forcing term in the governing equations, G_i , there are mainly two ways, i.e., the continuous (feedback) [9, 10] and discrete (direct) [11, 19] forcing term estimations. In this paper, the direct forcing term estimation shown in Fig.1 is adopted, because the larger time step (Δt) can be set up than the feedback forcing term estimation. We explain the proposed numerical approach in 2-D, but the extension to 3-D is straightforward.

For the forward Euler time integration, the forcing term can be determined by

$$G_i = \left[u_j \frac{\partial u_i}{\partial x_j} + \frac{\partial p}{\partial x_i} - \frac{1}{Re} \frac{\partial^2 u_i}{\partial x_j \partial x_j} \right]^n + \frac{\bar{U}_i^{n+1} - u_i^n}{\Delta t} \quad , \quad (8)$$

where \bar{U}_i^{n+1} denotes the linearly interpolated velocity by using U and u_{i+1} as shown in Fig.1. U is the boundary velocity, e.g., $U = 0$ for stationary solid media and $U = U_{move}$ for moving boundary, where U_{move} is the moving velocity. Namely, the external force is specified as the velocity components at next time step satisfy the relation, $u_i^{n+1} = \bar{U}_i^{n+1}$. The forcing term estimation is performed and the forcing term is added only to the grid points near the boundary. In this conventional forcing treatment, the pressure distributions near the boundary show the unphysical oscillations [19].

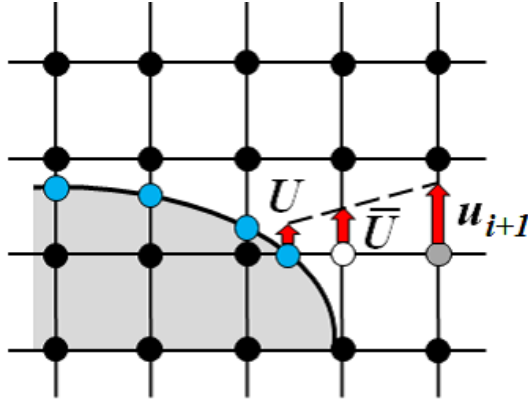


Figure 1: Discrete forcing treatment.

2.2.2 Seamless immersed boundary method

In order to remove aforementioned unphysical oscillations near the boundary, the seamless immersed boundary method was proposed [19]. In the seamless immersed boundary method, the forcing term is added not only to the grid points near the boundary but also to the grid points inside the boundary as shown in Fig.2. On the grid points near the boundary, the additional forcing term is estimated by the same procedure as the conventional direct forcing term estimation, Eq.(8). In the region inside the boundary, the forcing term is determined by satisfying the relation, $\bar{U}^{n+1} = U_{vb}$, where U_{vb} is the specified velocity, e.g., $U_{vb} = 0$ in stationary solid media and $U_{vb} = U_{move}$ for moving solid object.

Figure 3 shows the comparison of pressure field for flow around a circular cylinder with $Re = 40$ [19]. The conventional immersed boundary solution has the unphysical oscillation near the virtual boundary. On

the other hand, the seamless immersed boundary solution is very smooth even near the virtual boundary. It is found that the unphysical oscillation can be removed successfully.

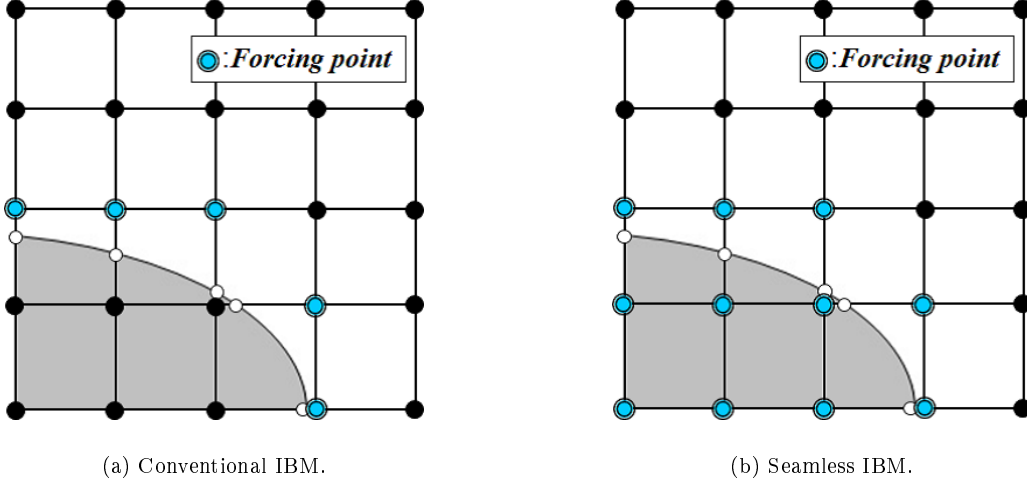


Figure 2: Grid points added forcing term.

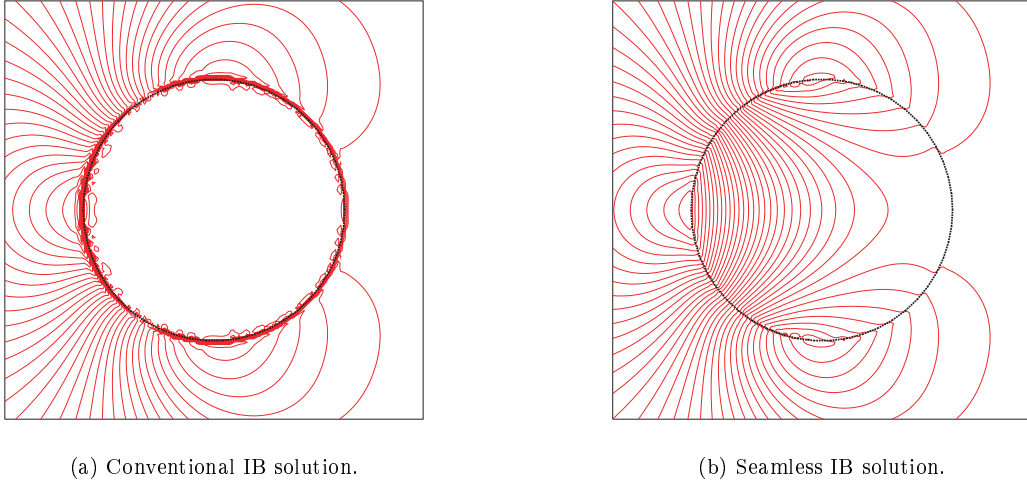


Figure 3: Comparison of pressure field ($Re = 40$) [19].

2.3 Seamless immersed boundary lattice Boltzmann method

Similar to the immersed boundary method for the incompressible Navier-Stokes equations, the lattice Boltzmann equation (2) is rewritten by

$$f_\alpha(\mathbf{x} + \mathbf{e}_\alpha \Delta t, t + \Delta t) - f_\alpha(\mathbf{x}, t) = -\frac{1}{\tau} \left[f_\alpha(\mathbf{x}, t) - f_\alpha^{(eq)}(\mathbf{x}, t) \right] + \Delta t \frac{w_\alpha \rho}{c_s^2} \mathbf{e}_\alpha \cdot \mathbf{g}(\mathbf{x}, t), \quad (9)$$

where $\mathbf{g}(\mathbf{x}, t)$ is the external forcing function defined by

$$\mathbf{g}(\mathbf{x}, t) = \frac{\bar{\mathbf{U}} - \mathbf{u}^*}{\Delta t}, \quad (10)$$

where $\bar{\mathbf{U}}$ is the specified velocity and \mathbf{u}^* denotes the tentative velocity at next time step [17].

In the seamless immersed boundary lattice Boltzmann method, this forcing function is added to the grid points not only near the boundary but also inside the boundary. On the grid points near the boundary, the specified velocity, $\bar{\mathbf{U}}$, is computed by linear interpolation between velocities on the virtual boundary and on the neighboring grid point as shown in Fig.1. On the grid points inside the boundary, the specified velocity is set as \mathbf{U}_{vb} , e.g., $\mathbf{U}_{vb} = 0$ for stationary solid media and $\mathbf{U}_{vb} = \mathbf{U}_{move}$ for moving solid object.

3 Computational Results

3.1 Validation of present approach

In order to validate the present approach, the flow around a circular cylinder is considered. The numerical solutions obtained by the present approach are compared with the conventional immersed boundary lattice Boltzmann solutions and the reference ones.

The computational domain is shown in Fig.4. The boundary of circular cylinder (circular cylinder surface) is expressed by the virtual boundary. The number of lattices is 840×440 (841×441 grid points), which is the resolution of 40 lattices per a diameter of circular cylinder. This lattice resolution ensures to obtain the precise physical quantities, e.g., the drag and lift coefficients, in the range of the Reynolds numbers ($Re = 40 \sim 200$). The initial flow is the uniform flow with $u = 0.1$, $v = 0.0$. The boundary conditions are $u = 0.1$, $v = 0.0$ for inflow boundary, $p = 1/3$ for outflow boundary and the extrapolation of macroscopic variables for side boundaries. Also, the velocity condition on the virtual boundary and inside the boundary is specified as the non-slip condition, $u = v = 0.0$.

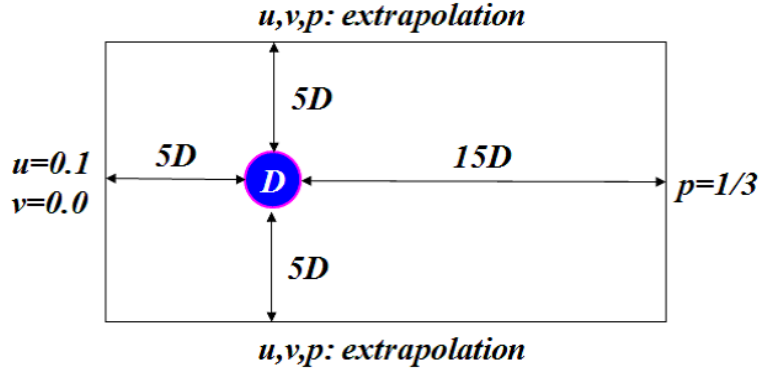


Figure 4: Computational domain and boundary conditions.

3.1.1 Steady flow

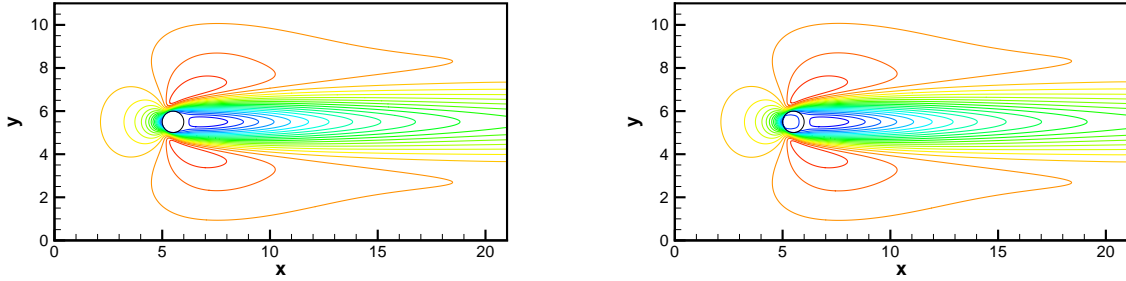
In this section, the steady state solution with $Re = 40$ is discussed. Figures 5 and 6 show the overall and closeup views of steady state velocity field (u -component) obtained by the present seamless and the conventional immersed boundary lattice Boltzmann methods, respectively. These velocity fields are almost the same. But, the velocity profiles inside a circular cylinder shown in Fig.6 are different. The seamless velocity field satisfies the velocity condition with machine zero, i.e., the order of 10^{-17} , whereas the conventional velocity field satisfies this condition with the order of 10^{-3} . Then, it is found that the present seamless approach can obtain the velocity field satisfying the velocity condition exactly.

Figures 7 and 8 show the overall and closeup views of steady state pressure field. In the overall view, the present seamless solution, Fig.7(a), and the conventional immersed boundary lattice Boltzmann solution, Fig.7(b), are in very good agreement with each other. It is found that the present pressure is distributed inside a circular cylinder. In the closeup view, however, the pressure distributions near the virtual boundary are different. The present solution represents the unique pressure on the virtual boundary (circular cylinder surface). And the pressure near the virtual boundary is very smooth. On the other hand, the pressure

obtained by the conventional immersed boundary lattice Boltzmann method distributes along the virtual boundary. Then, the important physical quantity, i.e., pressure on the circular cylinder surface, cannot determine precisely. Figure 9 shows the pressure along the center line. The present pressure is smooth. In the conventional immersed boundary solution, however, the pressure inside the virtual boundary becomes almost constant, so that the pressure jump near the virtual boundary appears. As a result, the conventional pressure distributes along the virtual boundary. Then, the quantitative values, such as the drag coefficient (Cd) and the lift coefficient (Cl), cannot estimate precisely in the conventional approach. Table 1 shows the comparison of Cd and Cl . In the conventional immersed boundary solution, Cd becomes higher than the present solution. It is found that the present seamless solution is close to the reference one [15] than the conventional immersed boundary solution. The drag and lift coefficients are estimated by integrating the external force,

$$Cd = \frac{-\int_s \rho \mathbf{g}_x(\mathbf{x}, t) ds}{1/2 \rho_\infty u_\infty^2 D}, \quad Cl = \frac{-\int_s \rho \mathbf{g}_y(\mathbf{x}, t) ds}{1/2 \rho_\infty u_\infty^2 D}, \quad (11)$$

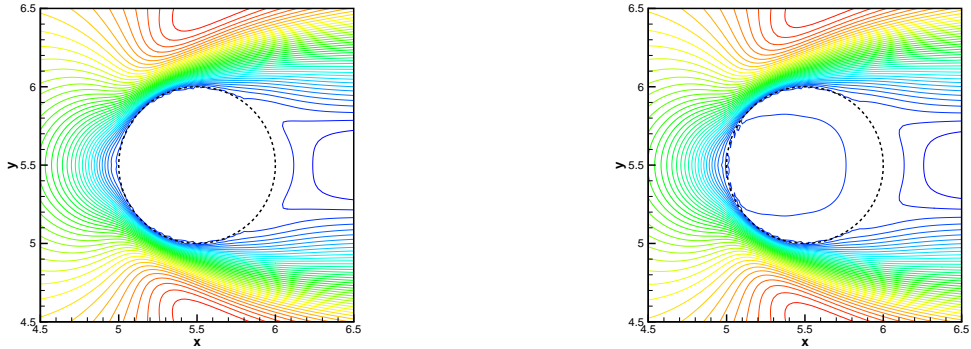
where the integration is carried out over the region with external force and $\mathbf{g}_x(\mathbf{x}, t)$ and $\mathbf{g}_y(\mathbf{x}, t)$ denote the external forcing function in x and y direction, respectively. The external force for the seamless immersed boundary method is determined to remain a circular cylinder stationary. Then, the reaction force can be regarded as the drag and lift.



(a) Seamless IB solution.

(b) Conventional IB solution.

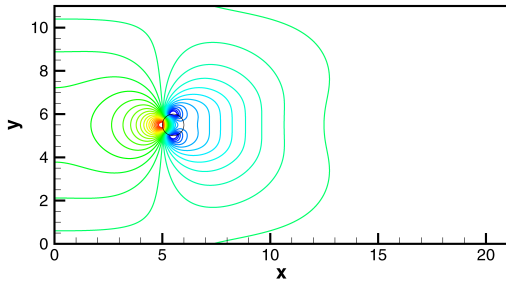
Figure 5: Overall view of velocity (u) field ($Re = 40$).



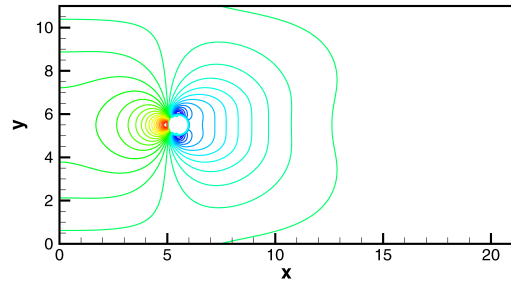
(a) Seamless IB solution.

(b) Conventional IB solution.

Figure 6: Closeup view of velocity (u) field ($Re = 40$).

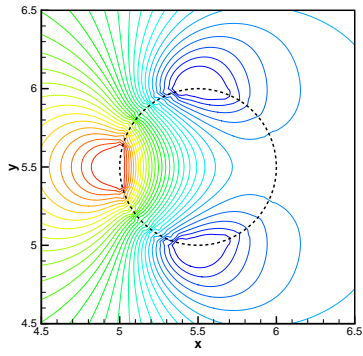


(a) Seamless IB solution.

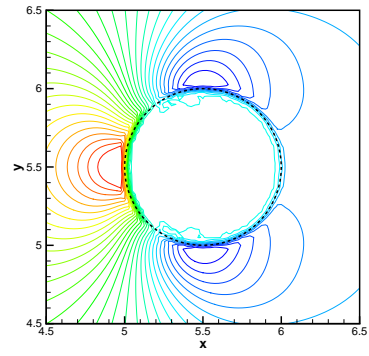


(b) Conventional IB solution.

Figure 7: Overall view of pressure field ($Re = 40$).

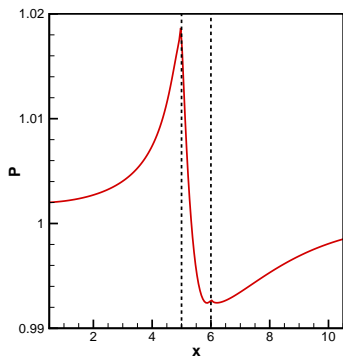


(a) Seamless IB solution.

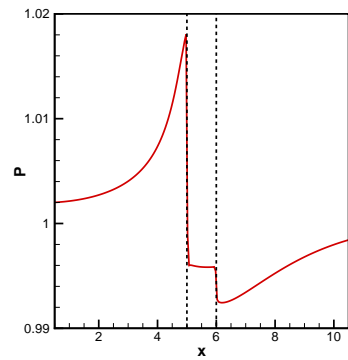


(b) Conventional IB solution.

Figure 8: Closeup view of pressure field ($Re = 40$).



(a) Seamless IB solution.



(b) Conventional IB solution.

Figure 9: Pressure profile along the center line ($Re = 40$).

Table 1: Comparison of Cd and Cl ($Re = 40$).

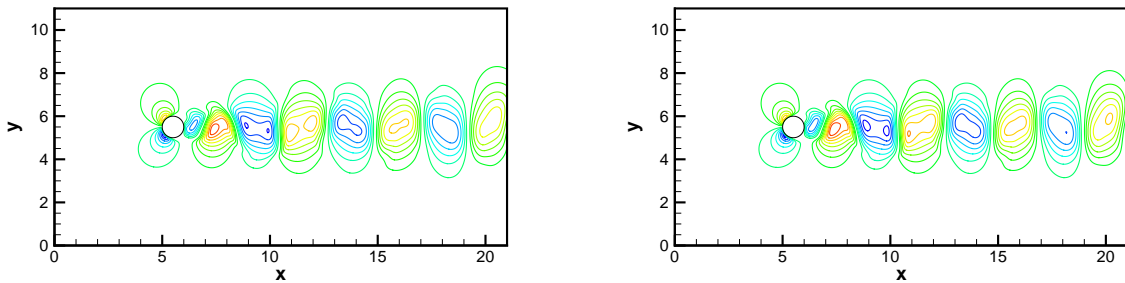
	Cd	Cl
Seamless IB	1.606	1.28×10^{-14}
Conventional IB	1.622	-1.79×10^{-15}
Niu et al.[15]	1.589	-

3.1.2 Unsteady flow

The unsteady flow with $Re = 200$ is presented in this section. Figures 10 and 11 show the snapshots of the velocity and pressure fields. In these overall views, both solutions can reproduce the vortex shedding clearly. Also both flow fields (velocity and pressure) are almost the same. However, in the closeup view of velocity shown in Fig.12, the velocity profiles inside the virtual boundary are different. The present velocity inside the virtual boundary becomes constant, but the conventional velocity distributes. The order of velocity inside the boundary is 10^{-17} for the seamless approach and 10^{-3} for the conventional approach.

For closeup view of pressure shown in Fig.13, it is found that the pressure obtained by the conventional immersed boundary method distributes along a circular cylinder surface. On the other hand, in the pressure obtained by the present seamless immersed boundary method, the smooth pressure field can be formed and the unique pressure value is obtained on the circular cylinder surface. Similar to steady flow, this discrepancy arises from the different pressure profiles near and inside the boundary, such as Fig.14. The conventional pressure profile is almost constant inside the boundary, so that the pressure jump appears near the boundary. On the other hand, the present pressure is very smooth. Figure 15 represents the time history of Cd and Cl . Table 2 shows the comparison of Cd , Cl and the Strouhal number St . Similar to the steady flow, the conventional immersed boundary solution gives the higher values of Cd in comparison with the present solution. It is found that the present solution is in good agreement with the reference one [25].

Therefore, it is concluded that the present seamless immersed boundary lattice Boltzmann method has the property satisfying the velocity condition on the boundary and inside the boundary, and removing the pressure jump near the boundary, so that the present approach gives the precise pressure near the boundary. Also, in the estimation of drag and lift, it is very easy to compute by integrating the additional external forces over the region with forcing.



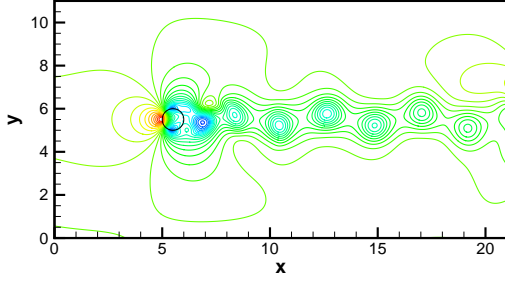
(a) Seamless IB solution.

(b) Conventional IB solution.

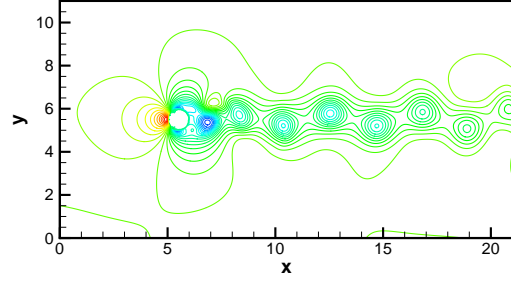
Figure 10: Snapshot of velocity (v) field ($Re = 200$).

3.2 Flow around an oscillating circular cylinder

In order to confirm the applicability of the present seamless approach to the moving boundary problem, the flow around an oscillating circular cylinder with $Re = 200$ is considered. The computational domain is shown in Fig.16. The circular cylinder in the uniform flow moves vertically as,

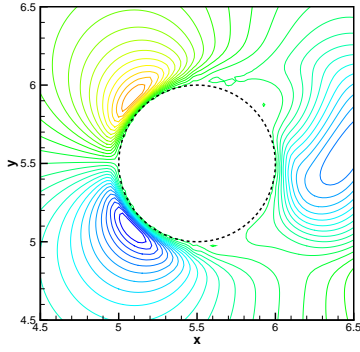


(a) Seamless IB solution.

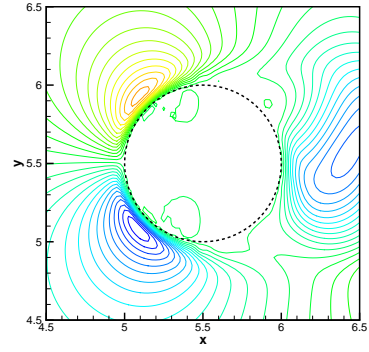


(b) Conventional IB solution.

Figure 11: Snapshot of pressure fields ($Re = 200$).



(a) Seamless IB solution.

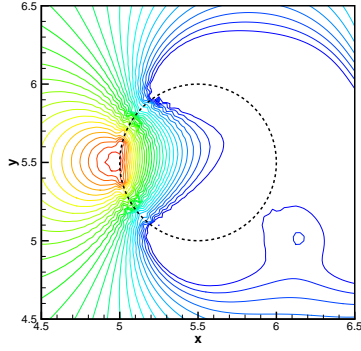


(b) Conventional IB solution.

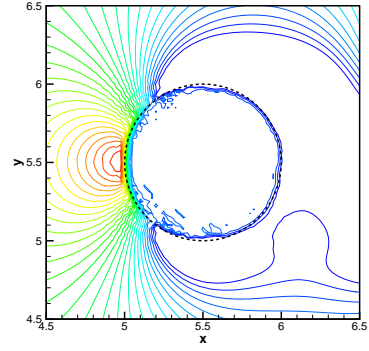
Figure 12: Closeup view of velocity (v) field ($Re = 200$).

Table 2: Comparison of Cd , Cl and St ($Re = 200$).

	Cd	Cl	St
Seamless IB	1.346 ± 0.0201	± 0.6557	0.202
Conventional IB	1.431 ± 0.0443	± 0.6654	0.204
Rosenfeld [25]	$1.329(\text{mean})$	± 0.674	0.197

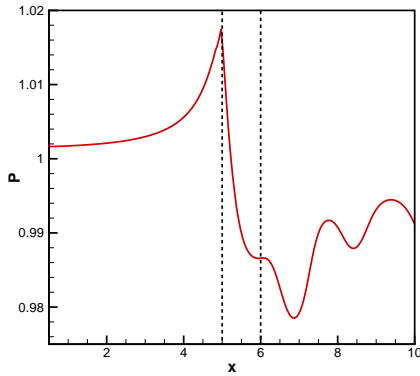


(a) Seamless IB solution.

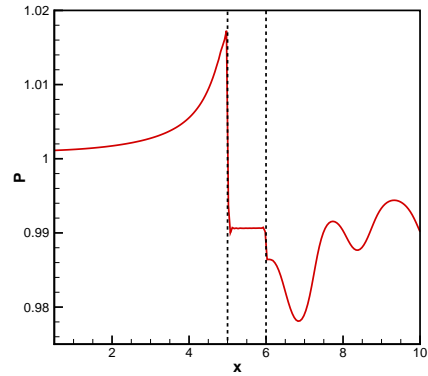


(b) Conventional IB solution.

Figure 13: Closeup view of pressure fields ($Re = 200$).

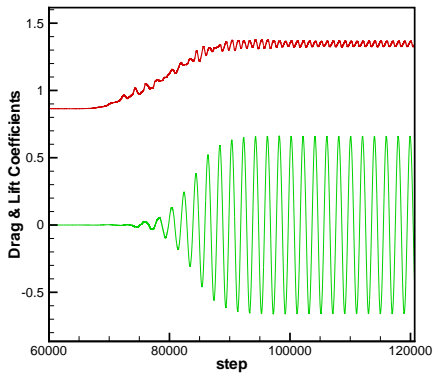


(a) Seamless IB solution.

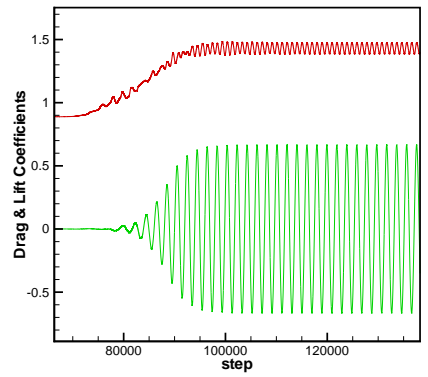


(b) Conventional IB solution.

Figure 14: Pressure profile along the center line ($Re = 200$).



(a) Seamless IB solution.



(b) Conventional IB solution.

Figure 15: Time history of Cd and Cl ($Re = 200$).

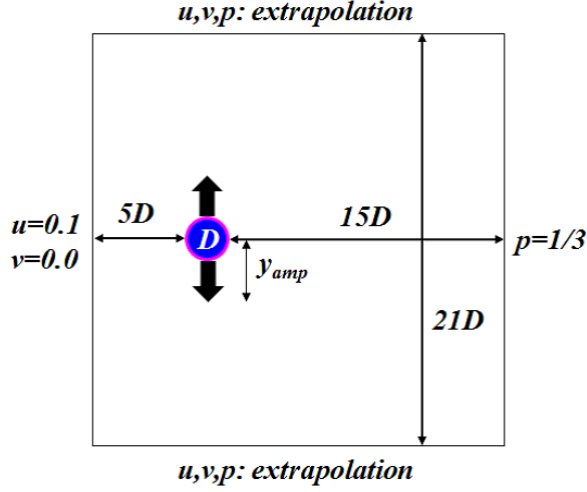


Figure 16: Computational domain and boundary conditions.

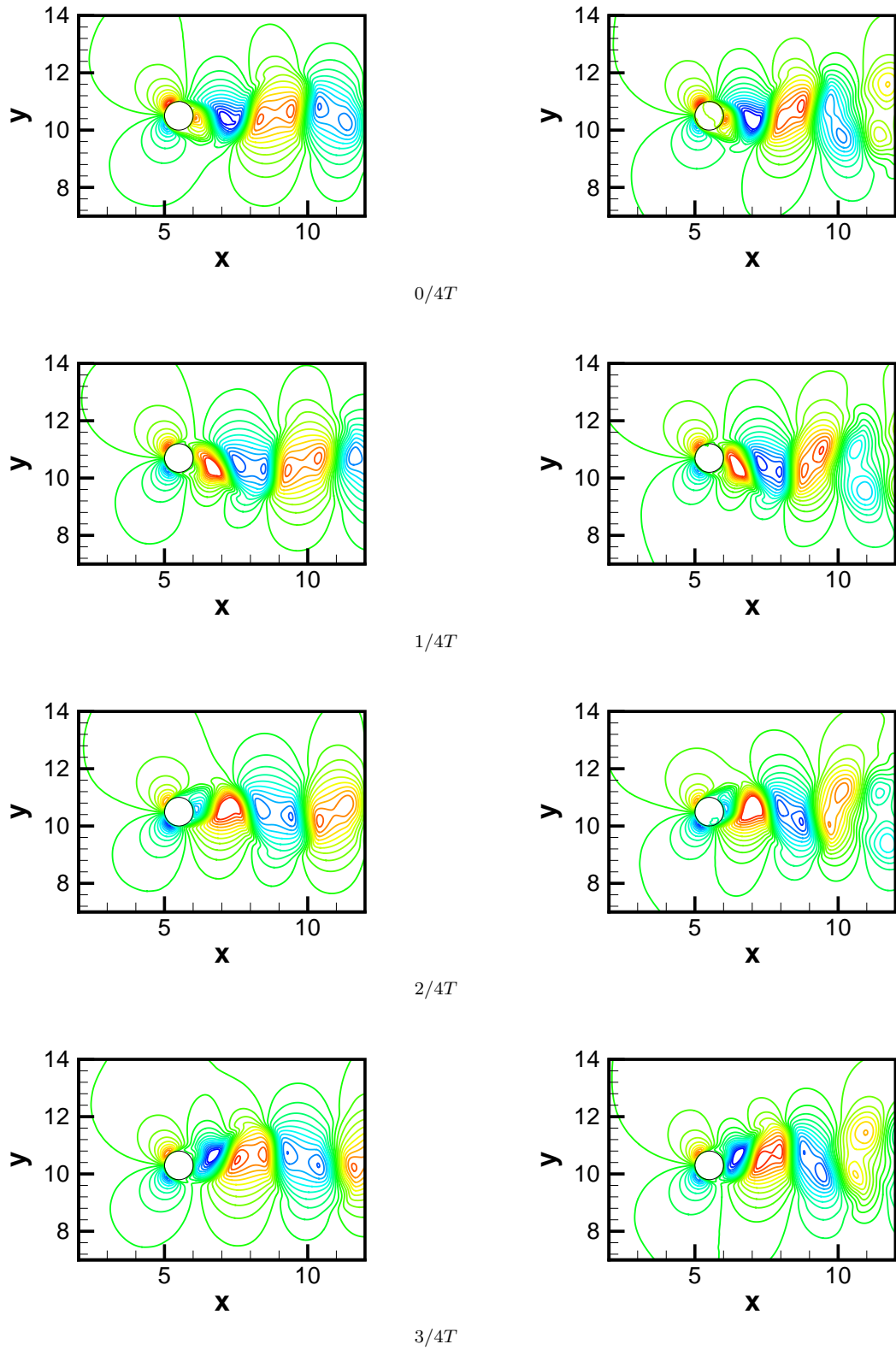
$$y(t) = y_0 + y_{amp} \sin(2\pi ft) , \quad (12)$$

where the amplitude is $y_{amp} = 0.2D$ and the non-dimensional oscillating frequency is $f = 0.2$. The initial location of circular cylinder is $(x_0, y_0) = (5.5D, 10.5D)$. The lattice resolution is 1680×1680 with 80 lattices per a diameter. The impulsive start determined by the uniform flow, $U = 0.1$, is adopted. On the inflow boundary, the velocity is fixed by the uniform flow and the pressure is imposed by the extrapolation. The velocity is extrapolated and the pressure fixed by $p = 1/3$ on the outflow boundary and the macroscopic pressure and velocity are extrapolated on the side boundaries. On the virtual boundary and inside the boundary, the moving circular cylinder velocity determined from Eq.(12) is imposed as the specified velocity for the immersed boundary method.

We compare the flow fields obtained by the seamless and conventional immersed boundary lattice Boltzmann methods at the 60th period from initial state. At this period, the periodic flow is reproduced. Figures 17 and 18 show the velocity (v) and pressure fields of one period ($0/4T, 1/4T, 2/4T, 3/4T$), respectively. T denotes the non-dimensional one period time. Both flow fields give the smooth wake, but in the conventional immersed boundary solution the wake becomes wider than the seamless immersed boundary solution. The closeup view of velocity and pressure is shown in Figs.19 and 20. Similar to the previous flow around a circular cylinder, the velocity condition inside the cylinder surface can be satisfied exactly in the seamless immersed boundary solution. On the other hand, the conventional immersed boundary solution shows the velocity distribution inside the boundary. Also, in the pressure the present seamless solution gives the very smooth pressure profile even near the cylinder surface at any time. In the conventional pressure, its profile distributes along the cylinder surface.

Figure 21 shows the time history of Cd and Cl . Table 3 represents the quantitative values of Cd , Cl , and St . The conventional immersed boundary results of Cd and Cl becomes higher than the seamless immersed boundary ones. In comparison with the reference result [26], the seamless immersed boundary results are in good agreement than the conventional ones. For the Strouhal number, St , the seamless and conventional immersed boundary results give the same value ($St = 0.2$) as the reference one. In this Reynolds number regime, it is reported that the lock-in phenomenon which the primary vortex shedding frequency has the same value with the oscillating frequency occurs [27]. It is found that both approaches reproduce the lock-in phenomenon.

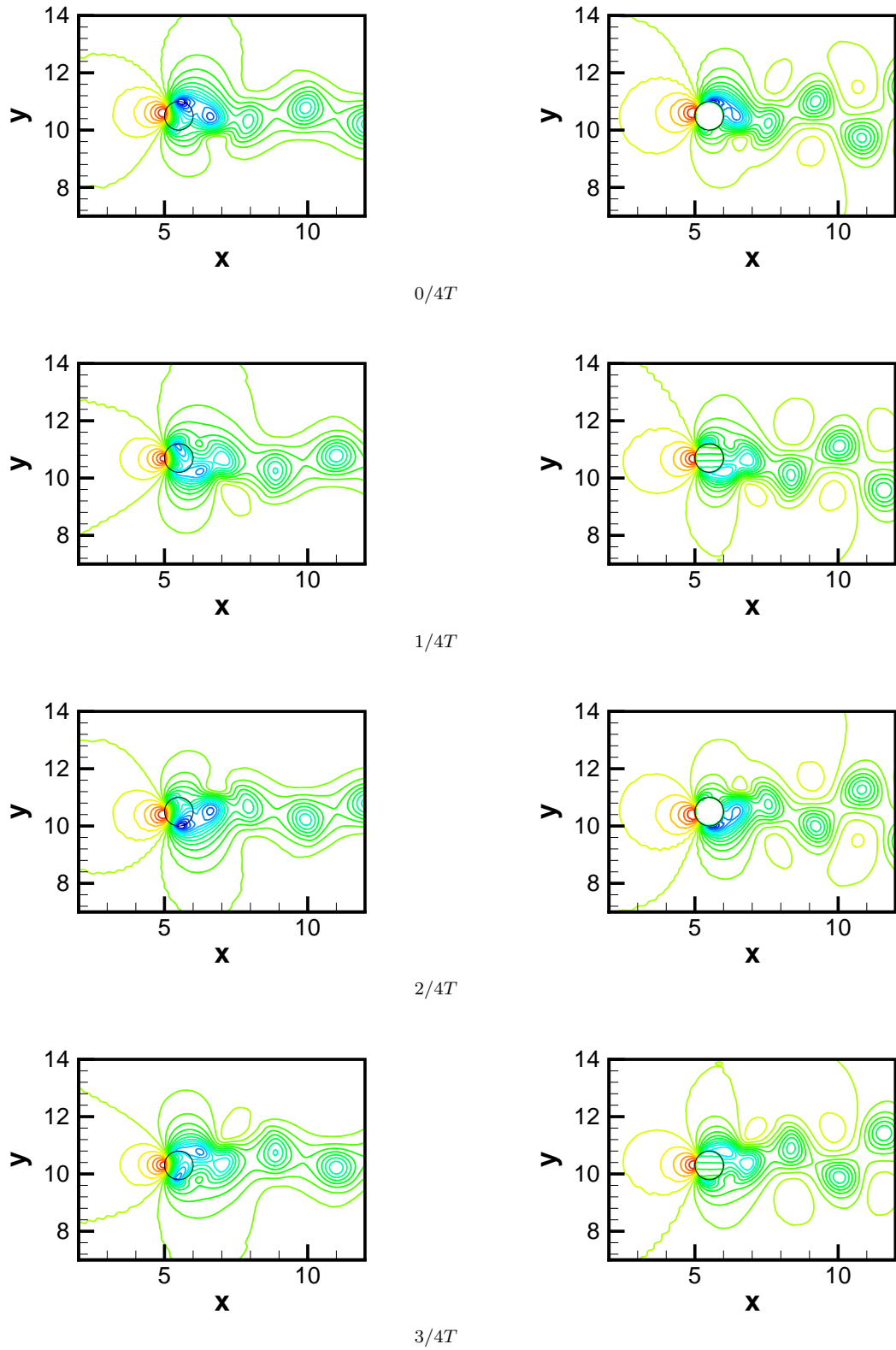
By taking account of the quantitative values, it is found that the seamless immersed boundary lattice Boltzmann method has the excellent computational property. Then, it is concluded that the present seamless immersed boundary lattice Boltzmann method is applicable to the flow simulation with moving boundary.



(a) Seamless IB solution.

(b) Conventional IB solution.

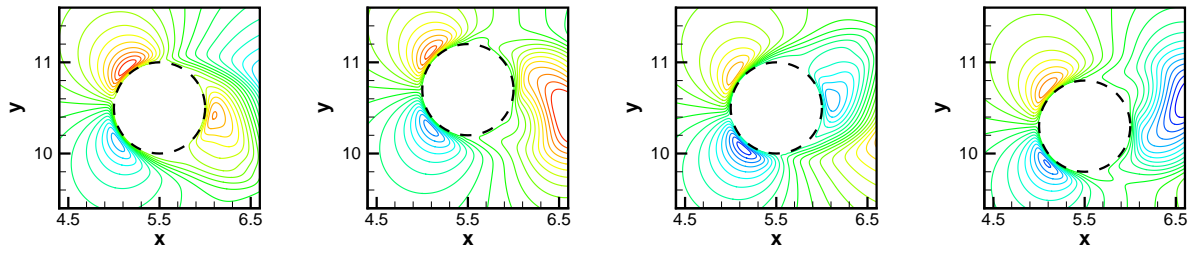
Figure 17: Snapshot of velocity (v) fields ($Re = 200$).



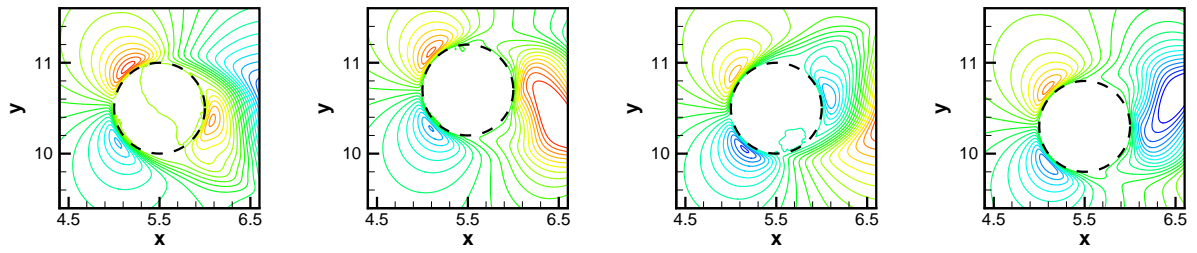
(a) Seamless IB solution.

(b) Conventional IB solution.

Figure 18: Snapshot of pressure fields ($Re = 200$).

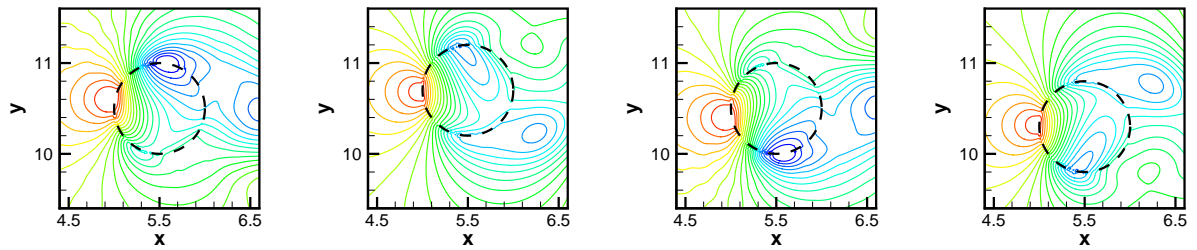


(a) Seamless IB solution.

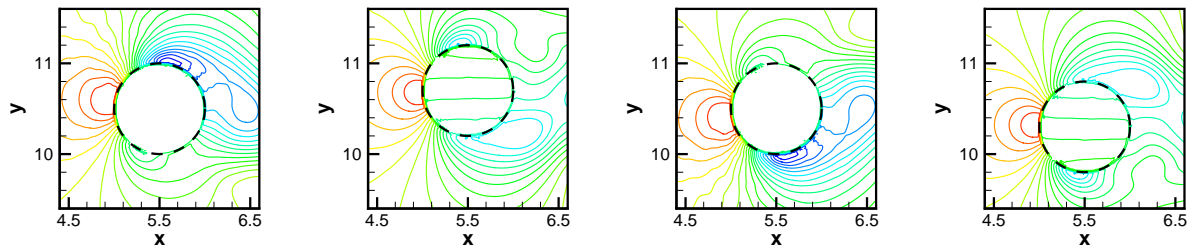


(b) Conventional IB solution.

Figure 19: Closeup view of velocity (v) fields ($Re = 200$).



(a) Seamless IB solution.



(b) Conventional IB solution.

Figure 20: Closeup view of pressure fields ($Re = 200$).

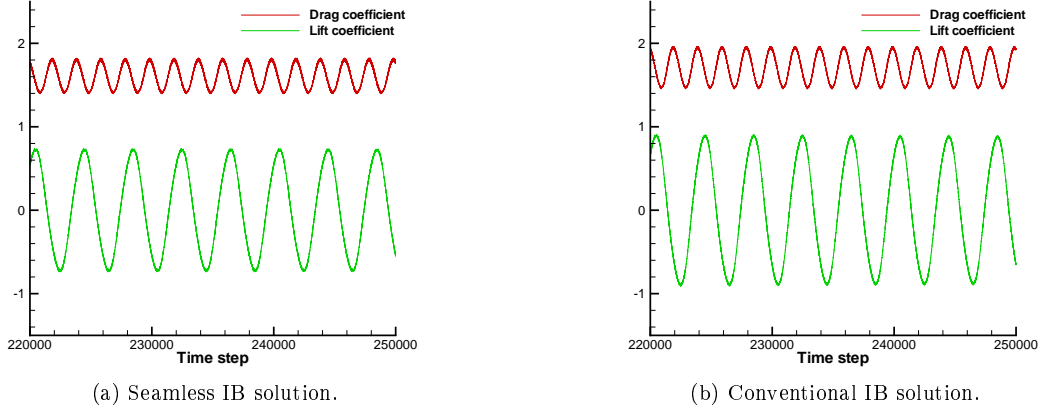


Figure 21: Time history of C_d and C_l ($Re = 200$).

Table 3: Comparison of C_d , C_l and St ($Re = 200$).

	C_d	C_l	St
Seamless IB	1.61 ± 0.20	± 0.72	0.20
Conventional IB	1.71 ± 0.23	± 0.88	0.20
Wu et al. [26]	1.58 ± 0.20	± 0.58	0.20

3.3 Flow around a moving circular cylinder in straight channel

In this section, we consider the flow around a moving circular cylinder in straight channel. Figure 22 shows the schematic of this problem. The number of lattices is 640×160 and the reference length is a diameter of circular cylinder (D) with 40 lattices.

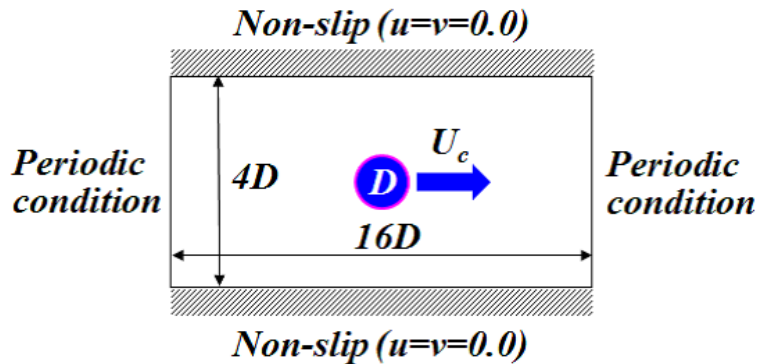


Figure 22: Computational domain and boundary conditions (Case-1).

A circular cylinder is set at the center of channel and is moving with $u = U_c = 0.1$, $v = 0.0$ and the upper and lower walls remain stationary, $u = v = 0.0$. On the right and left boundaries, the periodic boundary condition is imposed. And the initial pressure is set as $p = 1/3$. In order to compare the result, we consider the relatively equivalent flow field. As shown in Fig.23, a circular cylinder remains stationary and the upper and lower walls move with $u = U_w = -0.1$ and $v = 0.0$. The former is called Case-1 and the latter is

Case-2. The velocity condition on the virtual boundary and inside the boundary is specified as the non-slip condition, i.e., $u = U_c$, $v = 0.0$ for Case-1 and $u = v = 0.0$ for Case-2. The steady flow with $Re = 40$ based on a diameter of circular cylinder is considered. Then, two steady state solutions obtained by the present seamless immersed boundary lattice Boltzmann method are compared.

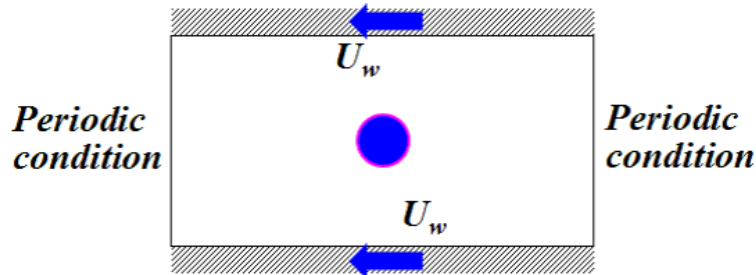


Figure 23: Computational domain and boundary conditions for Case-2.

Figures 24 and 25 show the velocity field (u and v) and pressure profile at the 31st period. At this period, the flow reaches to the almost steady state. In the velocity field, two cases, i.e., moving circular cylinder (Case-1) and moving walls (Case-2), show the same velocity profile. On the other hand, in the pressure field except inside the circular cylinder, both results are in very good agreement with each other. Also, the pressure near the circular cylinder is very smooth and seamless pressure can be obtained. Table 4 shows Cd and Cl obtained by Case-1 and Case-2. In the quantitative comparison, both results show the very good agreement with each other. Then, it is confirmed that both cases can obtain the equivalent flow field.

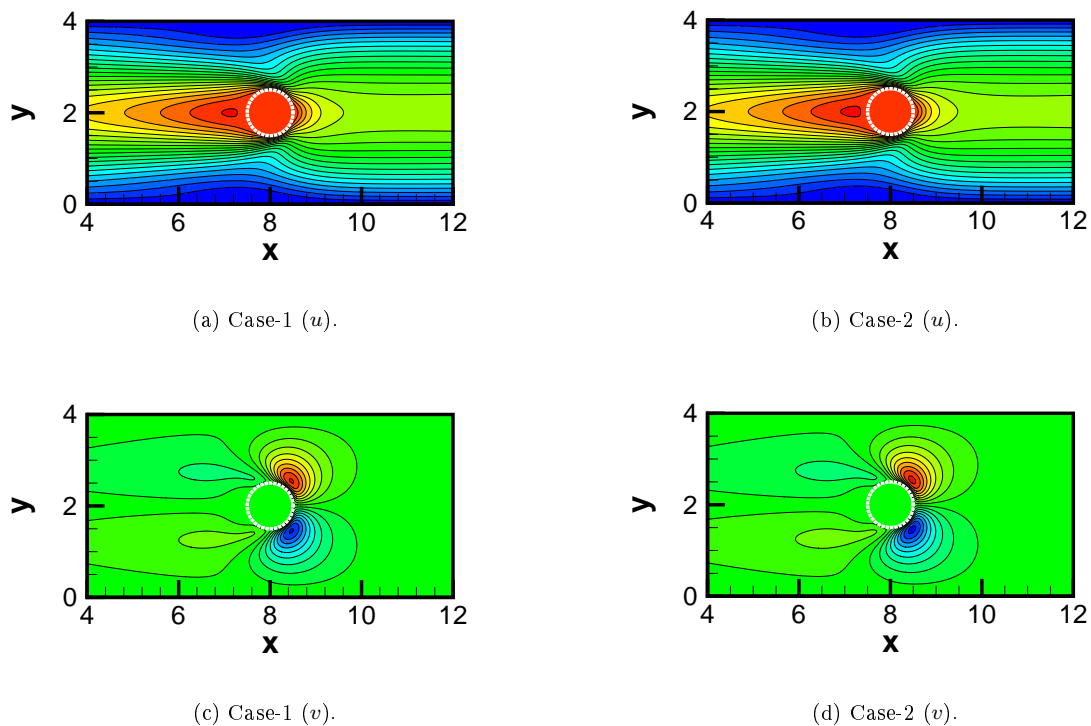


Figure 24: Comparison of velocity profile.

In the pressure profile inside the circular cylinder, however, the pressure is different. Therefore, the reference velocity ($U_c = 0.1$) is replaced by $1/10U_c$ in Case-1. Figure 26 shows the steady state pressure obtained

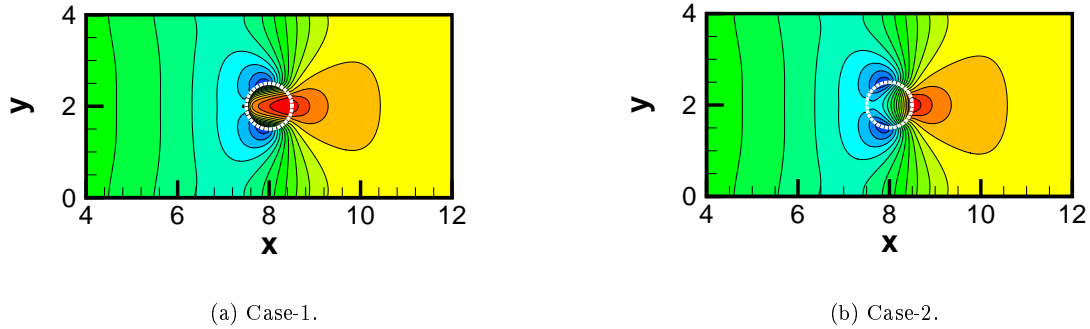


Figure 25: Comparison of pressure profile.

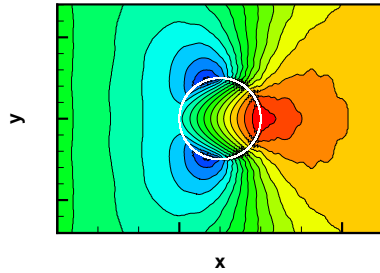


Figure 26: Pressure field with $U_c = 0.01$ in Case-1.

by $U_c = 0.01$. Due to the strict stability, there are some numerical oscillations, but the pressure inside the circular cylinder reproduces almost similar pressure profile obtained by Case-2 as shown in Fig.25(b). Then, it is confirmed that Case-1 gives the equivalent flow field including inside the circular cylinder by using the lower reference velocity.

As a result, for simulating the complicated flows with a moving boundary, it is concluded that the present seamless immersed boundary lattice Boltzmann method has the excellent computational property, i.e., the present approach can obtain the velocity satisfying the condition inside the boundary exactly and the smooth pressure without pressure jump near the boundary. Also, the present seamless approach can estimate the drag and lift very easily.

Table 4: Comparison of Cd and Cl .

	Cd	Cl
Case-1	0.73	1.4×10^{-14}
Case-2	0.72	3.0×10^{-15}

4 Conclusions

In this paper, the seamless immersed boundary lattice Boltzmann method is proposed. The present approach is an extension of the seamless immersed boundary method for the incompressible Navier-Stokes equations to the lattice Boltzmann equation. Similar to the seamless immersed boundary method, in the seamless immersed boundary lattice Boltzmann method, the external forcing function which satisfies the velocity condition on the virtual boundary and inside the boundary is added not only to the grid points near the

boundary but also to the grid points inside the boundary, so that the smooth and precise pressure profile near the boundary can be obtained. The present method is validated for the typical benchmark flows. As a result, it is confirmed that the present method gives the smooth pressure field without the unphysical oscillation and pressure jump near the virtual boundary. Also, in the present approach, the drag and lift can be estimated very easily by integrating the additional external forces. It is found that the present drag and lift are in good agreement with the reference ones. Then, it is concluded that the seamless immersed boundary lattice Boltzmann method is very versatile for simulating the complicated incompressible flows with a moving boundary.

References

- [1] D.R. Noble, S. Chen, J.G. Georgiadis, and R.O. Buckius. A consistent hydrodynamic boundary condition for the lattice Boltzmann method. *Phys. Fluids*, 7:203–209, 1995.
- [2] P. Ziegler. Boundary conditions for lattice Boltzmann simulation. *J. Stat. Phys.*, 71:1171–1177, 1993.
- [3] R. Mei and W. Shyy. On the finite difference-based lattice Boltzmann method in curvilinear coordinates. *J. Comput. Phys.*, 143:426–448, 1998.
- [4] T. Inamuro, M. Yoshino, and F. Ogino. A non-slip boundary condition for lattice Boltzmann simulation. *Phys. Fluids*, 7:2928–2930, 1995.
- [5] O. Filippova and D. Hanel. Grid refinement for lattice-BGK models. *J. Comput. Phys.*, 147:219–228, 1998.
- [6] R. Mei, L.-S. Luo, and W. Shyy. An accurate curved boundary treatment in the lattice Boltzmann method. *J. Comput. Phys.*, 155:307–329, 1999.
- [7] R. Mei, W. Shyy, D. Yu, and L.-S. Luo. Lattice Boltzmann method for 3-D flows with curved boundary. *J. Comput. Phys.*, 161:680–699, 2000.
- [8] C.S. Peskin and D.M. McQueen. A three-dimensional computational method for blood flow in the heart.I. immersed elastic fibers in a viscous incompressible fluid. *J. Comput. Phys.*, 81:372–405, 1989.
- [9] D. Goldstein, R. Handler, and L. Sirovich. Modeling a non-slip flow boundary with an external force field. *J. Comput. Phys.*, 105:354–366, 1993.
- [10] E.M. Saiki and S. Biringen. Numerical simulation of a cylinder in uniform flow: application of a virtual boundary method. *J. Comput. Phys.*, 123:450–465, 1996.
- [11] E.A. Fadlun, R. Verzicco, P. Orlandi, and J. Mohd-Yosof. Combined immersed-boundary finite-difference methods for three-dimensional complex simulations. *J. Comput. Phys.*, 161:35–60, 2000.
- [12] H. Nishida. Progress of current seamless virtual boundary method. *Computers & Fluids*, 45:59–63, 2011.
- [13] Z. Feng and E. Michaelides. The immersed boundary-lattice Boltzmann method for solving fluid-particle interaction problems. *J. Comput. Phys.*, 195:602–628, 2004.
- [14] Z. Feng and E. Michaelides. Proteus: a direct forcing method in the simulation of particulate flows. *J. Comput. Phys.*, 202:20–51, 2005.
- [15] X.D. Niu, C. Shu, Y.T. Chew, and Y. Peng. A momentum exchange-based immersed boundary-lattice Boltzmann method for simulating incompressible viscous flows. *Phys. Lett. A*, 354:173–182, 2006.
- [16] Y. Peng, C. Shu, Y.T. Chew, and X.D. Niu. Application of multi-block approach in the immersed boundary-lattice Boltzmann method for viscous fluid flows. *J. Comput. Phys.*, 218:460–478, 2006.
- [17] A. Dupuis, P. Chatelain, and P. Koumoutsakos. An immersed boundary-lattice Boltzmann method for the simulation of the flow past an impulsively started cylinder. *J. Comput. Phys.*, 227:4486–4498, 2008.
- [18] J. Wu and C. Shu. Implicit velocity correction-based immersed boundary-lattice Boltzmann method and its applications. *J. Comput. Phys.*, 228:1963–1979, 2009.
- [19] H. Nishida and K. Sasao. Incompressible flow simulations using virtual boundary method with new direct forcing terms estimation. *Computational Fluid Dynamics 2006*, pages 371–376, 2009.
- [20] H. Nishida and K. Tajiri. Numerical simulation of incompressible flows around a fish model at low Reynolds number using seamless virtual boundary method. *J. Fluid Science and Technology*, 4(3):500–511, 2009.
- [21] H. Nishida and K. Tajiri. Seamless virtual boundary method for incompressible flow simulation with heat transfer. *Trans. of the JSME*, 76(765):741–746, 2010. (in Japanese).

- [22] H. Nishida and A. Tanaka. Curvilinear seamless virtual boundary method for incompressible flow analysis. *Proc. of the 2nd Asian Symposium on Computational Heat Transfer and Fluid Flow*, pages 129–134, 2009.
- [23] Y.H. Qian, D. d’Humières, P. Lallemand, and L.-S. Luo. Lattice BGK models for Navier-Stokes equations. *Europhys. Lett.*, 17:479–483, 1992.
- [24] X. He and L.-S. Luo. Theory of the lattice Boltzmann equation: From Boltzmann equation to lattice Boltzmann equation. *Phys. Rev.*, E56:6811–6817, 1997.
- [25] M. Rosenfeld. Grid refinement test of time-periodic flows over bluff bodies. *Computers & Fluids*, 23:693–709, 1994.
- [26] G. Wu, B. Piao, and S. Kuroda. Development of cut cell method for incompressible fluid flows. *Proc. 18th Symp. on Computational Fluid Dynamics*, pages 1–5, 2004. (in Japanese).
- [27] S. Taneda. Visual study of unsteady separated flows around bodies. *Prog. Aerospace Sci.*, 17:287–348, 1977.